

OPEN ACCESS

Mechanics of the Ideal Double-Layer Capacitor

To cite this article: Charles W. Monroe 2020 *J. Electrochem. Soc.* **167** 013550

View the [article online](#) for updates and enhancements.



Mechanics of the Ideal Double-Layer Capacitor

Charles W. Monroe^{1,2,*}

¹Department of Engineering Science, University of Oxford, Oxford OX1 3PJ, United Kingdom

²The Faraday Institution, Harwell Campus, Didcot OX11 0RA, United Kingdom

The mechanical state within a parallel-plate electrolytic capacitor is examined by appending a local momentum balance to a quasielectrostatic theory that describes charge screening in both the electrolyte and the electrodes. A classical diffuse-double-layer model, which treats the capacitor's separator as a dilute electrolytic solution, is augmented to include metal electrodes, modelled as electron gases. When accounted for in this way, the electrodes are found to impact the interfacial capacitance significantly, as well as exerting compressive stress on the electrolyte. Nonlinear and quadratically perturbed theories are explored, the former around a single plate and the latter around the entire capacitor. Perturbation reveals several mechanical scaling laws generally applicable to capacitive metal/electrolyte interfaces. The two-plate model rationalizes the exponential decay of disjoining pressure between voltage-biased plates as their separation distance grows, as well as retrieving the well-known properties of a dielectric capacitor when the plate separation is small. This was Paper 1964 presented at the Dallas, Texas, Meeting of the Society, May 26–May 30, 2019.

© 2020 The Author(s). Published on behalf of The Electrochemical Society by IOP Publishing Limited. This is an open access article distributed under the terms of the Creative Commons Attribution 4.0 License (CC BY, <http://creativecommons.org/licenses/by/4.0/>), which permits unrestricted reuse of the work in any medium, provided the original work is properly cited. [DOI: 10.1149/1945-7111/ab6b04]



Manuscript submitted October 1, 2019; revised manuscript received January 8, 2020. Published February 21, 2020. *This Paper is part of the JES Focus Issue on Mathematical Modeling of Electrochemical Systems at Multiple Scales in Honor of Richard Alkire.*

Background

Among energy researchers, curiosity is growing about the mechanical responses that electricity can induce within electrolytic media. Our group has fleshed out a physico-chemical approach to such questions, based in classical equilibrium thermodynamics and the irreversible thermodynamics of Onsager¹ and de Groot.^{2,3} The theory extends in principle to electrodynamic mass-transport phenomena that violate the condition of local electroneutrality. Other frameworks that describe equilibrium in electrically polarised, non-neutral solid ionic conductors have been put forward in the past by Kornyshev and Vorotyntsev,⁴ and more recently by Latz et al.⁵ We have added to these earlier efforts by producing a general framework that also handles dissipative processes,⁶ encompassing Newman's now-standard electrolytic transport equations,⁷ but also accounting for mechanical dynamics via a coupled momentum balance. When applied to equilibrated systems, this dynamical model is consistent with Kornyshev–Vorotyntsev theory, as well as confirming results put forward by Latz.

Our model suggests that if a locally non-neutral electrolyte (i.e. a medium containing mobile charge carriers) is placed between blocking electrodes, and if a potential bias is applied between said electrodes, then double-layer formation is accompanied by a buildup of appreciable tensile stress in the bulk of the electrolyte relative to its edge.⁸ In hopes of elucidating the practical problem of the “critical current”, above which dendrites form in high-modulus ceramic lithium-ion conductors, I reported this observation in a recent seminar.⁹ Dr. Biggins, now of Corpus Christi College, Cambridge, expressed surprise that tension developed in the ceramic, since it is obvious that the oppositely charged plates of a traditional dielectric capacitor, being electrostatically attracted, will exert a compressive stress on their separating medium. He also rightly pointed out that our model did not consider any action whatsoever by the capacitor plates; nor did it address how stresses from the plates would compare to any stresses that might develop in the separator due to space charges near its boundaries.

The question whether bulk tensile stress due to interfacial space charging is physical raised particular concerns with us. At low voltage bias, the electrochemical portion of our modelling framework produces a description of electrode/electrolyte interfaces more or less identical to Gouy–Chapman theory;¹⁰ we merely used this electrochemical information to compute the local Lorentz body force

in a relatively uncontroversial way. Gouy–Chapman theory is well established and experimentally validated,¹¹ and has been used for a century to explain capacitance due to diffuse double layers at the boundaries of liquid electrolytes.

Despite its age, the theory of diffuse double layers continues to advance. Great strides have been made recently by Bazant et al.,¹² who created a variational analysis that addresses several pathological issues in the Gouy–Chapman model. Slightly later, Monroe et al. independently developed a similar variational method, using it to resolve specific problems that arise when applying Gouy–Chapman theory to parallel-plate electrolytic capacitors whose interelectrode spacing is small compared to the electrolyte's Debye length.¹³ When electrodes are very close together, an analysis employing a traditionally defined Debye length, based on the electrolyte's average concentration, leads standard Gouy–Chapman models to produce concentration distributions that fail to conserve mass. While resolving this mass-conservation issue, Monroe and colleagues solved a toy model of a capacitive “nano-gap”,^b which could produce a classical dielectric response in the limit of infinite electrolyte dilution. Thus we have available to us an electrochemical model that exhibits double-layer capacitance or classical dielectric behavior in appropriate limits of the electrolyte concentration.

This essay sets out to model the voltage distribution and mechanical forces in a parallel-plate capacitor separated by an electrolyte whose Debye length can be either much smaller than or much greater than the plate separation, which we respectively call the *electrolytic* and *dielectric* limits of the capacitor's response. We shall determine the stress distribution in both the electrode and the separator regions, and examine this result in the electrolytic and dielectric extremes. Primarily, we aim to deliver suitable responses to Dr. Biggins's insightful comments, within the context of the general framework developed by Goyal and Monroe.

Setup

Apparatus.—Consider the cell shown schematically in Fig. 1, wherein two freely sliding planar electrodes, each composed of the same electrochemically inert metal, are mounted on extremely stiff coil springs. The equilibrium separation of the electrodes in the empty cell is a fixed finite distance L , which we imagine to be an adjustable parameter of the apparatus. Before an experiment, a liquid

*Electrochemical Society Member.

^zE-mail: charles.monroe@eng.ox.ac.uk

^bCredit for phrasing this toy problem owes to the exceptional Prof. Alexander “Sasha” Kuznetsov (1938–2009), who posed it while appointed as Leverhulme Visiting Professor at Imperial College, London.

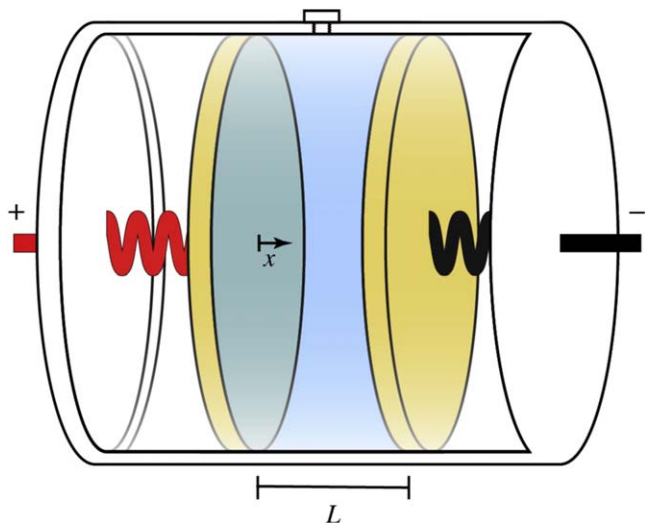


Figure 1. Schematic diagram of the hypothetical experimental apparatus. Two freely sliding cylindrical solid electrodes are inserted in a frictionless, electrically insulating, close-ended cylindrical shaft, acting as plugs that confine a fixed volume of liquid electrolyte. The positive and negative electrical contacts are wound to form coil springs, which are affixed to the ends of the shaft to balance any excess force owing to the presence of liquid or the application of voltage. In mechanical equilibrium without an applied voltage bias, the electrodes are separated by distance L .

electrolyte is added through a resealable access port to fill the interelectrode gap. The stiffness of the coil springs is such that L is negligibly affected by the hydrostatic force this added liquid exerts.

To run a thought experiment, we imagine connecting a potentiostat to the leads that protrude from the liquid-filled assembly and imposing a steady voltage bias between the electrodes. We expect this bias will cause charge accumulation in the metal at the electrode/electrolyte interfaces, which, being inert, block electrons from crossing. Since the ions in the liquid are mobile, and likewise cannot cross the interface to enter the metal, countercharges should simultaneously accumulate in the electrolyte near its two outer boundaries. In this way the whole device acts as a capacitor, whose differential capacitance can be measured by observing the change in surface charge on the metal with respect to the applied voltage bias, and should be determined by material properties peculiar to the electrodes and electrolyte. Because the charge distribution within the system exists in the presence of an electric field, applied voltage may also induce a mechanical force between the electrodes, which will be balanced by tension in the coil springs.

First we will observe the distributions of voltage, charge, and material that arise around one electrode of our hypothetical capacitor in response to the bias. A momentum balance will subsequently be exploited to elucidate the resultant mechanical forces. We shall solve this nonlinear problem exactly, but our solution requires a numerical computation of the potential at the metal/electrolyte interface. In the limit of small bias, a complete closed-form solution obtains. After these preliminaries we analyze the entire two-electrode system, also described by closed-form expressions when the voltage bias is small.

Governing equations.—Cauchy's equation expresses the local balance of momentum. No thermodynamic contradictions arise if the electric body force is included as a generation term within the momentum balance.⁶ Everywhere within a quasioleostatic stationary system like our capacitor, then,

$$\vec{0} = -\vec{\nabla} \cdot \vec{\sigma} + \vec{b}, \quad [1]$$

where $\vec{\sigma}$ is the Cauchy stress tensor and \vec{b} quantifies local body forces exerted by external fields.

Note that the sign of our Cauchy stress opposes the one used by practitioners of pure mechanics. For consistency with typical practices in classical chemical thermodynamics and standard chemical-engineering transport theory, we use a Cauchy stress $\vec{\sigma}$ that follows the sign convention employed in the canonical textbook by Bird, Stewart, and Lightfoot.¹⁴ In the BSL convention, the Cauchy stress is defined such that its average trace identifies with the external pressure p ,

$$\frac{1}{3}\text{tr}(\vec{\sigma}) = p; \quad [2]$$

and the deformation-stress tensor $\vec{\tau}$ is defined as the aspherical part of the total mechanical stress,

$$\vec{\tau} = \vec{\sigma} - p\vec{I}, \quad [3]$$

in which \vec{I} is the identity tensor. Any components of a traction \vec{t}_n that push on a surface with outward normal \vec{n} are defined to be positive, so that

$$\vec{t}_n = -\vec{n} \cdot \vec{\sigma} = -p\vec{n} - \vec{n} \cdot \vec{\tau}, \quad [4]$$

and the surface integral

$$\vec{f} = -\oint_{\partial V} \vec{n} \cdot \vec{\sigma} dS \quad [5]$$

produces the total external mechanical force \vec{f} that acts on a volume V bounded by surface ∂V .

Electromagnetic phenomena contribute to the body force \vec{b} . Analysis of the capacitor's mechanical state therefore requires an understanding of how space charge is distributed inside the metal electrodes, as well as within the electrolyte—we cannot use the standard postulates that the surface charges of metals lie in planes and that the potentials within bulk metals are uniform. Avoiding such assumptions is probably for the best anyway, because for them to hold, the Thomas–Fermi screening length of the metal must be negligible compared to the electrolyte's Debye length. These two characteristic lengths may be comparable, especially when electrolytes are moderately concentrated.¹⁵

Everywhere within the experimental apparatus, the electric displacement field, \vec{D} , is governed by Poisson's equation,

$$\vec{\nabla} \cdot \vec{D} = \rho_e, \quad [6]$$

in which ρ_e is the local excess charge density. When electrochemical equilibrium exists under a voltage bias—as in the electrolytic capacitor imagined here—charge density is usually taken to depend solely on the potential, but more complicated dependences can arise. For example, if materials in the capacitor were compressible, then the pressure distribution would impact both the charge-density distribution and the slab thickness, requiring Eqs. 1 and 6 to be solved simultaneously.

It should be emphasized that *Cauchy–Poisson analysis*, based on Eqs. 1 and 6, is far from new. These simultaneous governing equations are commonly applied in electrohydrodynamics, particularly when describing colloids or liquid suspensions.¹⁶ The novelty of Goyal and Monroe's work was its demonstration that Cauchy–Poisson analysis is consistent with Newman's electrochemical transport analysis, in the sense that no phenomenon is “double counted” if both theories are applied in tandem. Goyal and Monroe also dealt with the local constraints potentially imposed by thermodynamic state equations beyond the constitutive laws for electrochemical potential. For example, a local volumetric state equation derives from the Gibbs function and must be incorporated to ensure that the kinematic treatment of a material is consistent,¹⁷ as well as to permit the study of systems in which pressure, temperature, etc. substantially affect local carrier concentrations or volume strain. Including the state equation for volume also helps when enforcing conservation of carrier mass, a constraint we will apply later when exploring the two-electrode system.

Body-force constitutive laws.—The electrodes and electrolyte are assumed to be isotropic, so that the displacement field in medium k relates to its permittivity ϵ_k through

$$\vec{D} = \epsilon_k \vec{E}, \quad [7]$$

where \vec{E} represents the electric field. This relationship allows the body force in Eq. 1 to be written in more detail as

$$\vec{b} = \rho_e \vec{E} - \frac{1}{2} \vec{E} \cdot \vec{E} \vec{\nabla} \epsilon_k \quad [8]$$

(for simplicity, we disregard gravitational contributions to \vec{b}). Here $\rho_e \vec{E}$ is the Lorentz body force, and $-\frac{1}{2} \vec{E} \cdot \vec{E} \vec{\nabla} \epsilon_k$ is the Korteweg–Helmholtz body force due to changes in permittivity.¹⁸ Generally, a given material's permittivity can vary with respect to its local temperature, pressure, or composition. We neglect such effects for the moment, considering only the sharp spatial changes in ϵ_k that occur across junctions between distinct materials.

It is appropriate to adopt a quasielectrostatic assumption, so that $\vec{\nabla} \times \vec{E} \approx 0$; one can then write the standard relation

$$\vec{E} = -\vec{\nabla} \Phi \quad [9]$$

to define the electric potential Φ . When the electric field is conservative in this way, Eqs. 6 and 7 suffice to show that

$$\begin{aligned} \vec{b} &= \rho_e \vec{E} - \frac{1}{2} \vec{E} \cdot \vec{E} \vec{\nabla} \epsilon_k \\ &= \vec{\nabla} \cdot \left(\epsilon_k \vec{E} \otimes \vec{E} - \frac{1}{2} \epsilon_k \vec{E} \cdot \vec{E} \vec{I} \right) = \vec{\nabla} \cdot \vec{\sigma}_e. \end{aligned} \quad [10]$$

Thus electrostatic contributions to the body-force vector \vec{b} can be written equivalently as the convergence of a Maxwell stress tensor $\vec{\sigma}_e$, which facilitates analysis in some cases.

Introduction of the Maxwell stress defined in Eq. 10 allows the steady-state momentum balance to be written alternatively as

$$-\vec{\nabla} \cdot (\vec{\sigma} - \vec{\sigma}_e) = 0. \quad [11]$$

This equation can, in principle, be integrated directly to set up local relationships between the Cauchy stress and the electric field.

Mechanical constitutive laws.—The region of primary interest within the device depicted in Fig. 1 comprises two solid electrodes separated by a liquid electrolyte. In a steady state under a voltage bias, both solids and the liquid will be static. Throughout the liquid phase, this implies that the deformation stress in Eq. 3 vanishes, i.e. $\vec{\tau} = 0$. In the solid phases, $\vec{\tau}$ may vary; the electrodes can be idealized as purely elastic, so that there is a one-to-one relationship between $\vec{\tau}$ and the instantaneous deformation state.

As further idealizations, suppose that the electrolyte and electrodes both have very large bulk moduli, and also that the mass densities of both materials remain relatively constant with respect to carrier concentration. When considering Eq. 1, this allows one to suppose that any strain response due to stresses within the capacitor will be negligible. Thus the plate separation L (cf. Fig. 1) is independent of the capacitor's charge state, which decouples the momentum balance from the material and charge balances.

Electrochemical constitutive laws.—The decoupling of momentum and mass transport ensures that the electrical body forces depend solely on the distribution of voltage Φ , which will be determined below by solving isolated electrostatic problems. When phrasing these problems, we will think of the electrode interiors as ideal free-electron gases. Adopting a similar level of approximation, we take the electrolyte to be an ideal, nonreactive binary electrolytic solution, made up of a fully dissociated symmetric salt dissolved in a single dielectric-liquid solvent.

As discussed long ago by Rice,¹⁹ the Sommerfeld–Fermi theory implies that the local molar concentration of electrons in a metal, c_e , depends on the local potential as follows:

$$c_e = c_{\text{bulk}} \left[1 + \frac{2\gamma F(\Phi - \Phi_{\text{bulk}})}{3RT} \right]^{3/2}. \quad [12]$$

Here F is Faraday's constant, R the gas constant, and T the ambient temperature; c_{bulk} represents the free-electron concentration in the electrically neutral bulk metal, which state resides at Fermi energy $-F\Phi_{\text{bulk}}$. Also, the dimensionless Sommerfeld–Fermi parameter

$$\gamma = \frac{3m_e RT}{h^2 N_A} \left(\frac{8\pi}{3N_A c_{\text{bulk}}} \right)^{2/3}, \quad [13]$$

in which N_A , h , and m_e respectively represent Avogadro's number, Planck's constant, and the electron mass, expresses the thermal energy of the electron gas in units of its Fermi energy. Observe that γ is typically quite small: for gold, whose 98.0 M free-electron concentration at 25 °C is typical for metals under ambient conditions,²⁰ $\gamma = 0.007$. It follows from Eq. 12 and the definitions of c_{bulk} and Φ_{bulk} that the local excess charge density is

$$\begin{aligned} \rho_e &= -F(c_e - c_{\text{bulk}}) \\ &= -Fc_{\text{bulk}} \left\{ \left[1 + \frac{2\gamma F(\Phi - \Phi_{\text{bulk}})}{3RT} \right]^{3/2} - 1 \right\}. \end{aligned} \quad [14]$$

The metal's voltage response is determined by Eqs. 12 through 14 for values of Φ such that $c_e \geq 0$.^c

According to the Poisson–Boltzmann theory as applied most notably by Debye, Hückel, Gouy, Chapman, Derjaguin, Landau, Overbeek, and Verwey, as well as numerous others, the local concentrations of ions within a binary solution of a symmetric salt in a neutral solvent relate to the local potential through

$$c_{\pm} = c_{\text{ref}} \exp \left[\mp \frac{zF(\Phi - \Phi_{\text{ref}})}{RT} \right], \quad [15]$$

where z stands for the equivalent charge of cations; c_{ref} is the molar concentration of salt in an equilibrated, locally electroneutral solution, which state resides at reference potential Φ_{ref} . Due to the symmetry of the electrolyte, the excess charge density can be written compactly in the form

$$\rho_e = -2Fz c_{\text{ref}} \sinh \left[\frac{zF(\Phi - \Phi_{\text{ref}})}{RT} \right]. \quad [16]$$

Later on it will be convenient to work with the local average salt concentration, c , which we define as

$$c = \frac{c_+ + c_-}{2} = c_{\text{ref}} \cosh \left[\frac{Fz(\Phi - \Phi_{\text{ref}})}{RT} \right]. \quad [17]$$

Bazant et al. and Monroe et al. both showed that applying mass conservation as a constraint on free-energy minimization can cause c_{ref} to differ from the globally volume-averaged electrolyte concentration $\langle c \rangle$.

Geometrical considerations.—The apparatus schematized in Fig. 1 is intended to behave as a one-dimensional system. By design, all material properties within the cylindrical shaft vary only with respect to the spatial variable x . Edge effects are neglected, and the housing is taken to be electrically insulating, so that the electric potential within and between the electrodes varies only with x , and is invariant with respect to translation or rotation in the plane normal to x , which we call the y - z plane for convenience.

Given a potential distribution that satisfies Eqs. 6, 7, and 9, the stress distribution can be found relatively easily after a few steps of

^cAt any positive relative voltage $c_e > 0$; if $\Phi - \Phi_{\text{bulk}} < -3RT/2\gamma F$, however, c_e vanishes and ρ_e becomes constant, equalling Fc_{bulk} . We ignore this possible change in the metal's behavior at present because for a typical γ , the voltage threshold is well outside the stability window of a typical liquid electrolyte at room temperature (-5.5 V for $\gamma = 0.007$).

mechanical analysis that account for the one-dimensional nature of the apparatus. Since electric potential varies as $\Phi(x)$, definition 9 shows that the only nontrivial component of \vec{E} points in the x direction, so that $E_x(x)$, whereas $E_y = E_z = 0$. Further, Eq. 10 shows that the only nontrivial component of the body-force vector \vec{b} is aligned with the x axis, so that $b_x(x)$, whereas $b_y = b_z = 0$. Considerations of invariance in the y - z plane, along with an integration of the y and z components of Cauchy's Eq. 1, demonstrate that all shear stresses vanish. Thus the normal tensor components $\sigma_{xx}(x)$, $\sigma_{yy}(x)$, and $\sigma_{zz}(x)$ are the only nontrivial contributions to $\vec{\sigma}$.

Putting these considerations together with the restatement of Cauchy's equation in terms of Maxwell stress from Eq. 11, the x -momentum balance becomes

$$\frac{d\sigma_{xx}}{dx} = \frac{d}{dx} \left(\frac{1}{2} \epsilon_k E_x^2 \right). \quad [18]$$

This scalar equation is readily integrable to yield the single stress component $\sigma_{xx}(x)$.

The normal stress σ_{xx} is all that is needed to compute any net force between the capacitor's plates, which would be balanced by the coil springs shown in Fig. 1. When examining local property distributions, however, we find it more intuitive to cast results in terms of the thermodynamic pressure, p . The relationships between σ_{xx} and p are straightforward, but differ between the liquid and solid phases in the experimental apparatus. In the elastic solid-electrode phases, the body force $b_x(x)$ induces a uniaxial stress in the x direction; perpendicular to the electric field, one therefore has that $\sigma_{yy}(x) = \sigma_{zz}(x) = p^\theta$, where p^θ stands for the ambient pressure. It follows from Eq. 3 that the deformation stresses in the y - z plane vary as $\tau_{yy}(x) = \tau_{zz}(x) = p^\theta - p(x)$. Consistency of the definition in Eq. 2 demands that the deformation-stress tensor be traceless, however, so these y - z deformations must bring about a normal deformation stress in the x direction: $\tau_{xx} = -(\tau_{yy} + \tau_{zz})$. Thus the gauge normal stress is three times the gauge pressure,

$$\sigma_{xx}(x) - p^\theta = 3[p(x) - p^\theta] \quad (\text{electrodes}). \quad [19]$$

In the liquid phase, $\vec{\tau} = \vec{0}$ uniformly, so the stress tensor must be spherical. It follows that

$$\sigma_{xx}(x) = \sigma_{yy}(x) = \sigma_{zz}(x) = p(x) \quad (\text{electrolyte}), \quad [20]$$

i.e. all three normal stress components match the total pressure.

The Semi-Infinite Capacitive Interface

First we analyze a plane interface at position $x = 0$, with metal at positions $x < 0$ (which we may call the *left* side of the interface) and electrolyte at positions $x > 0$ (the *right*). A bias $\Delta\Phi$ relative to the bulk-solution potential Φ_{ref} is applied, holding the Fermi level of the metal far to the left at $\Phi_{\text{bulk}} = \Phi_{\text{ref}} + \Delta\Phi$. In this situation Poisson's equation governs the field everywhere, and reduces to nonlinear ordinary differential equations in both media. It will be convenient below to use the transformation

$$\phi = \frac{F(\Phi - \Phi_{\text{ref}})}{RT} \quad [21]$$

to cast all voltages dimensionlessly; for example, the dimensionless bias is denoted $\Delta\phi$. We suppose the metal has constant permittivity ϵ_M (at $x < 0$) and the liquid has permittivity ϵ (at $x > 0$).

In the metal, whose potential is labeled with a subscript L, for "left", Eqs. 6, 7, 9, and 14 combine to give

$$\lambda_M^2 \gamma \frac{d^2 \phi_L}{dx^2} = \left[1 - \frac{2}{3} \gamma (\Delta\phi - \phi_L) \right]^{3/2} - 1. \quad [22]$$

Here the Thomas-Fermi length λ_M is defined in terms of the bulk free-electron concentration far to the left of the interface, $c_{\text{bulk}} = c_{-\infty}$, as

$$\lambda_M = \sqrt{\frac{\epsilon_M RT}{F^2 \gamma c_{-\infty}}}. \quad [23]$$

Equation 22 can be reduced to a first-order ordinary differential equation by asserting that the local electric field in the metal, $E_L = -d\Phi_L/dx$, depends exclusively on the local potential, so that $E_L(\phi_L)$. Direct integration, adding the requirement that the bulk Fermi level of the metal should correspond to a condition with no space charge, i.e. $E_L(\Delta\phi) = 0$, shows that

$$E_L(\phi_L) = \frac{RT \text{sgn}(\Delta\phi - \phi_L)}{F \gamma \lambda_M} \times \sqrt{\frac{6}{5} \left\{ \left[1 - \frac{2}{3} \gamma (\Delta\phi - \phi_L) \right]^{5/2} - 1 \right\} + 2\gamma (\Delta\phi - \phi_L)}. \quad [24]$$

The sign function in this result selects the appropriate branch of the square root, assuming radicals are naturally positive. Branches were chosen based on the physical argument that there should be a positive surface charge on the metal when the interfacial potential is below $\Delta\phi$.

Through Eqs. 6 and 16, the electric potential in the liquid is governed by the classical nonlinear Poisson-Boltzmann equation

$$\lambda^2 z \frac{d^2 \phi}{dx^2} = \sinh(z\phi), \quad [25]$$

where the Debye length λ is

$$\lambda = \sqrt{\frac{\epsilon RT}{2F^2 z^2 c_{\text{ref}}}}. \quad [26]$$

Again, reduction of order allows direct integration of Eq. 25 to get the field $E = -d\Phi/dx$:

$$E(\phi) = \frac{2RT}{Fz\lambda} \sinh\left(\frac{1}{2}z\phi\right). \quad [27]$$

This was derived assuming that $E(0) = 0$, because the liquid far to the right of the interface is electroneutral.

The potential is continuous across the interface between metal and liquid, requiring that $\phi(0) = \phi_L(0) = \phi_0$. Also stability requires the field to change monotonically as it crosses the interface, so the interfacial potential ϕ_0 must lie between 0 and $\Delta\phi$. Introduce the bounded parameter $0 \leq \alpha \leq 1$ to represent the fraction of the total potential drop on the liquid side of the interface: $\phi_0 = \alpha \Delta\phi$. Because conservation of charge requires the electric displacement to be continuous across the interface, then,

$$\epsilon_M E_L(\alpha \Delta\phi) = \epsilon E(\alpha \Delta\phi), \quad [28]$$

or, inserting Eqs. 24 and 27,

$$\begin{aligned} & \frac{3}{5} \left\{ \left[1 - \frac{2}{3} \gamma (1 - \alpha) \Delta\phi \right]^{5/2} - 1 \right\} + \gamma (1 - \alpha) \Delta\phi \\ &= \left(\frac{\gamma}{z} \cdot \frac{1 - \alpha_0}{\alpha_0} \right)^2 [\cosh(z\alpha \Delta\phi) - 1], \end{aligned} \quad [29]$$

in which we have squared both sides to eliminate the sign function and the square root, and then used a half-angle formula to remove the square of the hyperbolic sine. This provides an implicit equation whose solution establishes the function $\alpha(\Delta\phi)$.

The partition coefficient α is bounded between 0 and 1, so Eq. 29 can be solved readily via a numerical binary search. Note that a regular perturbation analysis of Eq. 28 was used to identify the parameter

$$\frac{1}{\alpha_0} = 1 + \sqrt{\frac{2z^2\epsilon c_{\text{ref}}}{\gamma\epsilon_M c_{-\infty}}}, \quad \text{or} \quad \alpha_0 = \frac{\frac{\epsilon_M}{\lambda_M}}{\frac{\epsilon}{\lambda} + \frac{\epsilon_M}{\lambda_M}}, \quad [30]$$

which quantifies how material properties partition the bias in the limit as $\Delta\phi$ tends to 0. (Note that ϵ/λ has units of capacitance per area.) Figure 2 shows the fraction of the voltage drop across the liquid electrolyte as a function of voltage bias.

To provide a sense of how a typical electrode and electrolyte partition the bias voltage, consider a 0.05 M solution of sodium chloride in water ($\epsilon = 80\epsilon_0$), adjacent to gold. Kornyshev and Vorotyntsev suggest that for gold, $\epsilon_M \approx \epsilon_0$. (Kornyshev et al. state more precisely that $1 < \epsilon_M/\epsilon_0 < 10$ for most metals, and that experiments suggest the relative permittivity is usually closer to 1.¹⁵) This makes the Thomas–Fermi length 0.59 Å—about a twentieth of the Debye length (13.7 Å). For this interface $\alpha_0 = 0.23$, so most of the potential drop occurs on the metal side. Fits of differential capacitance data, such as the canonical results presented by Grahame,²¹ might provide further insight into ϵ_M and λ_M . Absent precise values, we will present robust methods that allow computation of the partition coefficient $\alpha(\Delta\phi)$ for any α_0 between 0 and 1. Note that for an ideal electrolyte, α_0 goes to unity at infinite dilution, and reaches a minimum at the salt’s solubility limit.

One useful property of the ideal metal/solution interface is its differential areal capacitance \tilde{C} , found by differentiating the surface charge density on the metal, Σ_M , with respect to the total bias voltage:

$$\tilde{C} = \frac{d\Sigma_M}{d\Delta\Phi} = \frac{F\epsilon_M}{RT} \frac{dE_L|_{\phi_L=\alpha\Delta\phi}}{d\Delta\phi} = \frac{F\epsilon}{RT} \frac{dE|_{\phi=\alpha\Delta\phi}}{d\Delta\phi}. \quad [31]$$

Here the last equality follows from displacement continuity, Eq. 28. Equation 27 can be inserted to get

$$\tilde{C} = \frac{\epsilon}{\lambda} \cosh\left(\frac{1}{2}z\alpha\Delta\phi\right) \cdot \alpha \left(1 + \frac{d \ln \alpha}{d \ln \Delta\phi}\right), \quad [32]$$

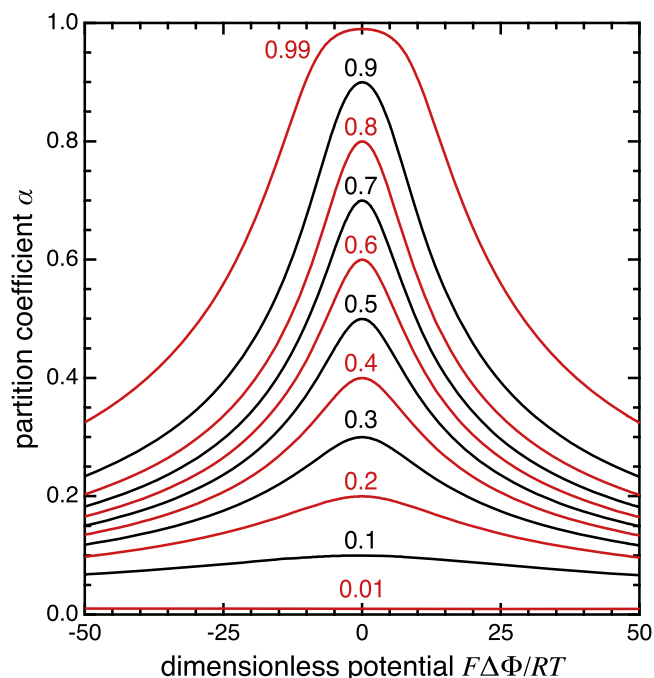


Figure 2. Partitioning of voltage drop to the liquid as a function of total voltage bias given an electrode with Sommerfeld–Fermi parameter $\gamma = 0.007$, for electrode/electrolyte pairs with null-bias partition coefficients α_0 ranging from 0.01 to 0.99.

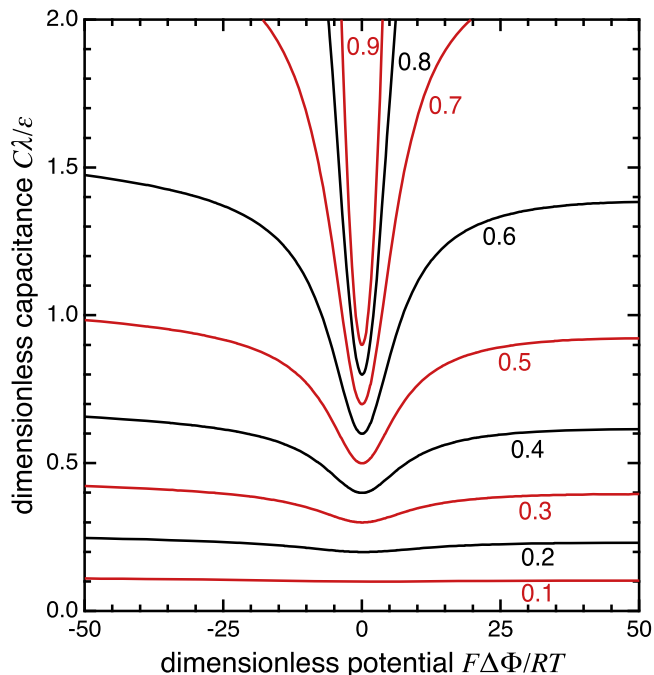


Figure 3. Specific capacitance as a function of interfacial voltage drop for null-bias partition coefficients α_0 ranging from 0.1 to 0.9, in a system whose electrode has Sommerfeld–Fermi parameter $\gamma = 0.007$.

wherein implicit differentiation of Eq. 29 demonstrates that

$$\left[\alpha \left(1 + \frac{d \ln \alpha}{d \ln \Delta\phi} \right) \right]^{-1} = 1 + \frac{\frac{\gamma}{z} \left(\frac{1-\alpha_0}{\alpha_0} \right)^2 \sinh(z\alpha\Delta\phi)}{1 - \left[1 - \frac{2}{3}\gamma(1-\alpha)\Delta\phi \right]^{3/2}}. \quad [33]$$

Albeit unwieldy, this is straightforward to compute once $\alpha(\Delta\phi)$ is known from Eq. 29.

Figure 3 presents the interfacial capacitance as a function of bias voltage for interfaces with a range of partition coefficients. The responses look generally like predictions of the Gouy–Chapman–Stern theory²²—the capacitance saturates as the bias reaches large magnitudes, and dips near the potential of zero charge. Unlike the traditional Stern correction, however, the metal’s screening behavior causes the capacitance signatures to be asymmetric between the high-bias extremes.

The potential distribution can be found through Eqs. 24 and 27, noting that the potential at $x = 0$ is $\alpha\Delta\phi$. Implement the method of Chapman¹⁰ by separating and integrating Eq. 27 to find

$$x(\phi) = \lambda \ln \left[\frac{\tanh\left(\frac{1}{4}z\alpha\Delta\phi\right)}{\tanh\left(\frac{1}{4}z\phi\right)} \right]; \quad 0 < \frac{\phi}{\Delta\phi} \leq \alpha, \quad [34]$$

which describes the region to the right of the interface. Following a similar procedure, separate and integrate Eq. 24 to show that on the left of the interface (that is, when $\phi_L/\Delta\phi > \alpha$),

$$\frac{x(\phi_L)}{\lambda_M} = \int_{1-\sqrt{1-2\gamma(1-\alpha)\Delta\phi/3}}^{1-\sqrt{1-2\gamma(\Delta\phi-\phi_L)/3}} \frac{(1-u)du}{u\sqrt{1-\frac{4}{3}u+\frac{2}{3}u^2-\frac{2}{15}u^3}}, \quad [35]$$

where a change of variable has cast the integral in a numerically amenable form.^d Exemplary potential distributions across the

^dNB: A closed-form solution for $x(\phi_L)$ was found in terms of incomplete elliptic integrals, but the expression was cumbersome enough, and incomplete elliptic integrals sufficiently obscure, that we instead chose to compute the function numerically.

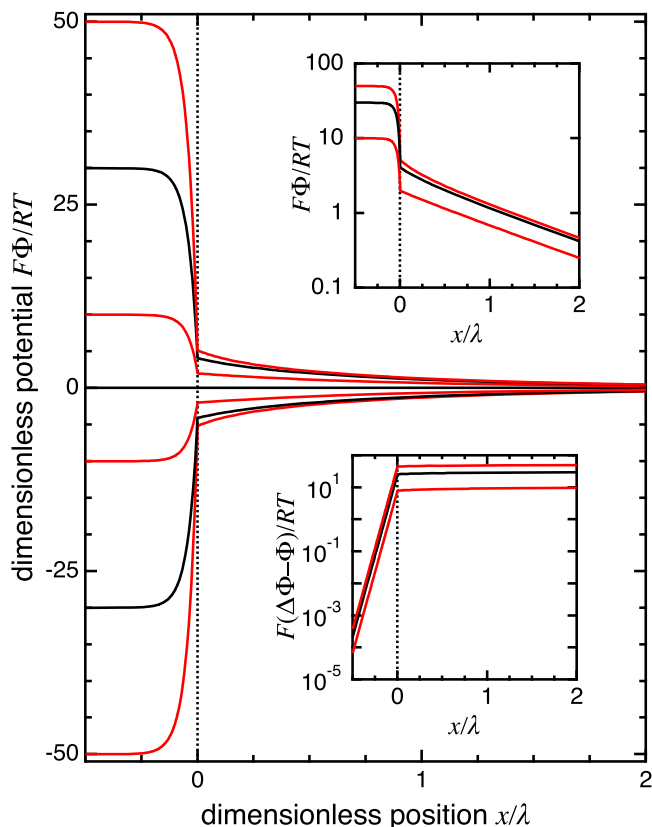


Figure 4. Potential distribution around a gold/0.05 M aqueous NaCl interface ($\gamma = 0.007$, $\alpha_0 = 0.23$, $\lambda_M/\lambda = 0.042$) as a function of bias voltage. The insets put the positive-bias data on appropriately shifted semi-log plots to demonstrate that screening manifests as an approximately exponential decay toward the bulk potential on either side of the interface.

interface between gold and 0.05 M aqueous sodium chloride ($\gamma = 0.007$, $\alpha_0 = 0.23$, $\lambda_M/\lambda = 0.042$) are shown in Fig. 4.

Now that the electrical problem is solved, we can proceed with the mechanical analysis. The Korteweg–Helmholtz contribution to normal stress can be considered in isolation, because the only spatial change in permittivity is a step from ϵ_M to ϵ as x crosses zero. Since the dividing surface that separates the metal from the liquid is infinitesimally thin, and therefore contains no charge density, one has that

$$-\frac{1}{2} \int_{-\infty}^x E^2 \frac{d\epsilon_k}{dx} dx = \frac{1}{2} \Sigma_M^2 \left(\frac{1}{\epsilon} - \frac{1}{\epsilon_M} \right) H(x), \quad [36]$$

in which $H(x)$ represents the Heaviside step function. Korteweg–Helmholtz force accounts for a discontinuity in $\sigma_{xx}(x)$ at $x = 0$, because Eqs. 28 and 36 combine to show that

$$\frac{1}{2} \Sigma_M^2 \left(\frac{1}{\epsilon} - \frac{1}{\epsilon_M} \right) = \frac{1}{2} [\epsilon E^2(\alpha \Delta\phi) - \epsilon_M E_L^2(\alpha \Delta\phi)], \quad [37]$$

in which the terms on the right clearly relate to the Maxwell-stress component seen on the right of Eq. 18. With Eqs. 36 and 37 in hand, x -momentum balance 18 can be integrated and combined with Eqs. 19 and 20 to find the pressure distribution in terms of the field. Assuming that $p = p^\theta$ far to the left of the interface, the pressure distribution becomes

$$p(x) - p^\theta = \begin{cases} \frac{1}{6} \epsilon_M E_L^2; & x < 0, \\ \frac{1}{2} \epsilon E^2; & x > 0. \end{cases} \quad [38]$$

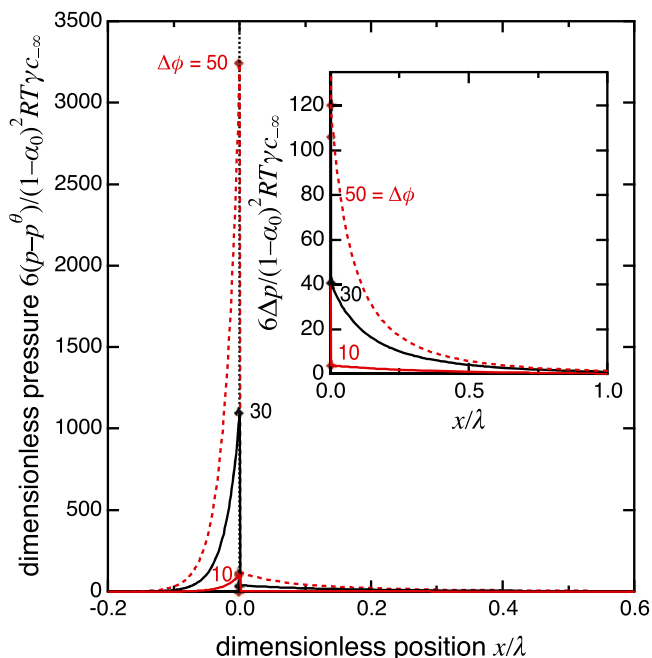


Figure 5. Pressure distribution around a gold/0.05 M aqueous NaCl interface ($\gamma = 0.007$, $\alpha_0 = 0.23$, $\lambda_M/\lambda = 0.042$) at three bias voltages. Peak pressures on either side of the interface are emphasized with diamonds. The inset details the distribution on the electrolyte side of the interface.

Insertion of the fields from Eqs. 24 and 27 into Eq. 38 yields explicit formulas for the pressure distribution, parameterized by the bias $\Delta\phi$, the Sommerfeld–Fermi parameter γ , the null-bias partition coefficient α_0 , and the length ratio λ_M/λ :

$$\frac{6(p - p^\theta)}{(1 - \alpha_0)^2 RT \gamma c_{\infty}} = \begin{cases} \frac{\left[\frac{1 - \frac{2}{3}\gamma(\Delta\phi - \phi_L)}{3} \right]^{5/2} - 1 + \frac{5}{3}\gamma(\Delta\phi - \phi_L)}{\frac{5}{6}\gamma^2(1 - \alpha_0)^2}; & \alpha < \frac{\phi_L}{\Delta\phi} \leq 1, \\ \frac{3\alpha_0\lambda_M}{(1 - \alpha_0)\lambda} \cdot \left[\frac{\sinh(\frac{1}{2}z\phi)}{\frac{1}{2}z\alpha_0} \right]^2; & 0 \leq \frac{\phi}{\Delta\phi} < \alpha. \end{cases} \quad [39]$$

Here, the scaling of $p - p^\theta$ was selected to make the peak dimensionless pressure on the metal side exactly equal $\Delta\phi^2$ in the limit of small bias.

We can now provide a clear response to Dr. Biggins' first comment. Figure 5 shows how the pressure distribution around the interface varies as the metal is raised to increasingly positive voltages. (The distributions remain qualitatively similar when the bias is negative.) Although the bulk of the electrolyte is under tensile stress relative to its edge, the bulk actually resides at ambient pressure. Due to attraction between the back-to-back space-charge layers in the metal and electrolyte, a compressive force concentrates in a very thin region near the interface, whose width is of the order of $\frac{1}{2}(\lambda_M + \lambda)$ and does not change appreciably with bias. The maximum gauge pressures on both sides of the interface are directly proportional to $\Delta\phi^2$ when the bias is small, and remain of the order of $\Delta\phi^2$ at higher voltages. On the liquid side, the scale of the peak pressure differs from the metal's by a factor of three times the dielectric-constant ratio, since $\alpha_0\lambda_M/(1 - \alpha_0)\lambda = \epsilon_M/\epsilon$.

Semi-Infinite Analysis at Low Bias

Approximate solutions of the nonlinear model can provide a clearer quantitative understanding, delivering scaling laws that show

the orders of the forces concentrated around the double layer. We begin by analyzing the semi-infinite metal-electrolyte interface in the limit where the dimensionless bias $\Delta\phi$ is small—an effort that will help to illustrate methods for tackling the two-electrode problem.

A regular perturbation analysis can be performed with respect to the dimensionless bias by letting

$$\begin{aligned}\phi_L(x) &= \Delta\phi\phi_L^{(1)}(x) + \Delta\phi^2\phi_L^{(2)}(x) + O(\Delta\phi^3) \\ \phi(x) &= \Delta\phi\phi^{(1)}(x) + \Delta\phi^2\phi^{(2)}(x) + O(\Delta\phi^3) \\ p(x) &= p^0 + \Delta\phi p^{(1)}(x) + \Delta\phi^2 p^{(2)}(x) + O(\Delta\phi^3).\end{aligned}\quad [40]$$

Functions $\phi_L^{(1)}$, $\phi^{(1)}$, $\phi_L^{(2)}$, and $\phi^{(2)}$ are expected to be $O(1)$. A key result of this section will be to uncover the natural scale of pressure at the interface by analyzing the perturbed momentum balance.

Perturbation of Eq. 38 requires that $p^{(1)} = 0$, in line with the prior observation that interfacial pressure scales as $\Delta\phi^2$ (cf. Fig. 5). The first significant electrostatic contribution to pressure is

$$p^{(2)}(x) = \begin{cases} \frac{1}{6}RT\gamma c_{-\infty} \left(\lambda_M \frac{d\phi_L^{(1)}}{dx} \right)^2; & x < 0, \\ RTz^2 c_{\text{ref}} \left(\lambda \frac{d\phi^{(1)}}{dx} \right)^2; & x > 0. \end{cases}\quad [41]$$

First-order electrical information suffices to establish the pressure distribution. The electrostatic analysis will still be carried out to second order, however, to explore how capacitance varies with bias.

The left side of the interface is governed by Eq. 22 and the right satisfies Eq. 25. By ansatz, voltages ϕ and ϕ_L are both of the order of $\Delta\phi$. Thus, if the total bias is small, then the right side of Eq. 22 can be approximated by Maclaurin expansion in $\Delta\phi - \phi_L$, as

$$\begin{aligned}\left[1 - \frac{2}{3}\gamma(\Delta\phi - \phi_L)\right]^{3/2} - 1 \\ = -\gamma(\Delta\phi - \phi_L) + \frac{1}{6}\gamma^2(\Delta\phi - \phi_L)^2 + O(\Delta\phi^3),\end{aligned}\quad [42]$$

and the right side of Eq. 25 by Maclaurin expansion in ϕ , as

$$\sinh(z\phi) = z\phi + O(\Delta\phi^3).\quad [43]$$

In the linear perturbation, the potential on the left side of the interface satisfies

$$\lambda_M^2 \frac{d^2\phi_L^{(1)}}{dx^2} - \phi_L^{(1)} = -1,\quad [44]$$

and at second order, it follows

$$\lambda_M^2 \frac{d^2\phi_L^{(2)}}{dx^2} - \phi_L^{(2)} = \frac{1}{6}\gamma(1 - \phi_L^{(1)})^2.\quad [45]$$

Because the hyperbolic sine is odd, the perturbed Poisson–Boltzmann equation becomes inhomogeneous only at orders three and higher; the electrolyte's potential satisfies

$$\lambda^2 \frac{d^2\phi^{(k)}}{dx^2} - \phi^{(k)} = 0\quad [46]$$

up to the quadratic perturbation ($k \in \{1, 2\}$).

Nonlinear differential governing equations become linear in their perturbations, which makes the application of boundary conditions more straightforward than in the prior section. Equations 44 to 46 satisfy far-field conditions

$$\lim\phi_L^{(k)}(x) = \delta_{1k}\Delta\phi \text{ and } \lim\phi^{(k)}(x) = 0,\quad [47]$$

where δ_{ij} is the Kronecker delta, equal to 1 if $i = j$ and 0 otherwise, as well as interfacial matching conditions

$$\phi_L^{(k)}(0) = \phi^{(k)}(0) \text{ and } \epsilon_M \frac{d\phi_L^{(k)}}{dx} \Big|_0 = \epsilon \frac{d\phi^{(k)}}{dx} \Big|_0.\quad [48]$$

Being linear, these boundary conditions hold at any order of perturbation k .

The problem established by governing Eqs. 44 through 46 subject to the boundary conditions in Eqs. 47 and 48 is solved by

$$\begin{aligned}\phi_L &= [1 - (1 - \alpha_0)e^{x/\lambda_M}]\Delta\phi - \frac{1}{18}\gamma(1 - \alpha_0)^2 \\ &\quad \times (\alpha_0 + 1 - e^{x/\lambda_M})e^{x/\lambda_M}\Delta\phi^2 + O(\Delta\phi^3); \quad x < 0, \\ \phi &= \alpha_0 e^{-x/\lambda}\Delta\phi - \frac{1}{18}\gamma(1 - \alpha_0)^2\alpha_0 e^{-x/\lambda}\Delta\phi^2 \\ &\quad + O(\Delta\phi^3); \quad x > 0.\end{aligned}\quad [49]$$

Here the zero-bias partition coefficient α_0 , introduced earlier to simplify Eq. 30, arises naturally from the matching boundary conditions.

These potential distributions allow one to identify the interfacial capacitance through Eq. 31,

$$\tilde{C} = \tilde{C}_0 \left[1 - \frac{1}{9}\gamma(1 - \alpha_0)^2\Delta\phi \right] + O(\Delta\phi)^2,\quad [50]$$

in which the new parameter

$$\tilde{C}_0 = \frac{\epsilon}{\lambda}\alpha_0 = \frac{\epsilon_M}{\lambda_M}(1 - \alpha_0) = \left(\frac{1}{\epsilon_M/\lambda_M} + \frac{1}{\epsilon/\lambda} \right)^{-1}\quad [51]$$

quantifies the total areal capacitance of the interface at zero bias. The equality on the right emphasizes that \tilde{C}_0 puts in series the individual areal capacitances due to charge screening on the metal and electrolyte sides of the interface. Insertion of the parameters appropriate for 0.05 M aqueous NaCl next to gold ($\alpha_0 = 0.23$, $\epsilon/\lambda = 52 \mu\text{Fcm}^{-2}$) shows that $\tilde{C}_0 = 12 \mu\text{Fcm}^{-2}$, about a quarter of what one would expect from linear Gouy–Chapman theory, which considers the electrolyte alone.

Equation 50 indicates a possible route by which the Sommerfeld–Fermi parameter could be measured experimentally: γ determines the slope of the differential capacitance at the potential of zero charge. If the value of $\gamma = 0.007$ for gold is correct, one would expect this linear variation of C with bias to be very weak, however. Observe that the finite slope of $\tilde{C}(\Delta\phi)$ at zero bias shows that the commonly assumed equivalence between the potential of zero charge and the global differential-capacitance minimum cannot be drawn. This raises a general philosophical question about how the potential of zero charge can be established experimentally, since most electrode/electrolyte interfaces are presumably both nonideal and inherently charged.

Insertion of the first-order terms from Eq. 49 into Eq. 41 shows that the second-order contribution to the pressure distribution is

$$p^{(2)}(x) = \begin{cases} p_0 \sqrt{\frac{(1 - \alpha_0)\lambda}{\alpha_0\lambda_M}} e^{2x/\lambda_M}; & x < 0, \\ 3p_0 \sqrt{\frac{\alpha_0\lambda_M}{(1 - \alpha_0)\lambda}} e^{-2x/\lambda}; & x > 0. \end{cases}\quad [52]$$

The analysis has thus led us to a new parameter p_0 , which expresses the natural scale of the gauge pressure:

$$p_0 = \frac{1}{6\sqrt{\epsilon_M\epsilon}} \left(\frac{RT\tilde{C}_0}{F} \right)^2.\quad [53]$$

For the 0.05 M aqueous NaCl/gold interface, $p_0 = 20 \text{ kPa}$. Bearing in mind that the interfacial gauge pressure scales as $p_0\Delta\phi^2$ (cf. Eq. 40 et seq.), this shows an appreciable increase with bias: $30 \text{ Pa} \cdot \text{mV}^{-2}$. Further recalling that $\alpha_0\lambda_M/(1 - \alpha_0)\lambda = \epsilon_M/\epsilon = 1/80$, Eq. 52 shows the peak pressure on the gold side to rise at $0.27 \text{ kPa} \cdot \text{mV}^{-2}$, whereas the aqueous peak pressure grows at $10 \text{ Pa} \cdot \text{mV}^{-2}$.

Equations 52 and 53 expose several mechanical rules of thumb applicable to any electrochemical interfaces that support space

charging. First, as we set out to show, the gauge stress in the double layer is always compressive, regardless of the sign of the bias. Second, stress peaks at the interface, and falls off exponentially to the ambient pressure on either side, with a characteristic length half of that phase's screening length. Third, pressure at the interface scales with the square of the total interfacial capacitance, and inversely with the geometric mean of the bulk permittivities on either side—interfaces with higher total capacitance experience much higher peak pressures. Fourth, the peak stress is highest on the side with lower permittivity, and lower on the opposing side; the ratio of these maxima scales with the bulk permittivity ratio, and the difference between them owes to the Korteweg–Helmholtz force. Last, the mechanical impact of double-layer charging can be significant, despite the fact that it emerges only at second order in the governing equations—a bias of just 19 mV produces about 1 atmosphere of gauge pressure on the gold side of an aqueous NaCl/gold interface.

The Parallel-Plate Double-Layer Capacitor

Although they led to several useful qualitative observations, the semi-infinite analyses—both nonlinear and regularly perturbed—left one of our key motivating questions unresolved. We originally sought to query the dielectric extreme of electrolyte behavior, to check consistency of the present model with the well-known expression for the force between plates in a planar dielectric capacitor. One should be able to explore this regime analytically by taking $\lambda \rightarrow \infty$, but the analysis up to now cannot produce sensible results in that limit because the plate separation L was not brought into account.

Setup.—We shall finally consider the entire system from Fig. 1, with two plane metal/electrolyte interfaces, one at position $x = 0$ and another at $x = L$. One metal electrode, which we shall still call the *left* electrode, denoting its potential ϕ_L , resides at positions $x < 0$. The other metal electrode resides at positions $x > L$; we shall call this the *right* electrode, whose potential is ϕ_R . We assume that the two electrodes are composed of the same metal, so that both have the same permittivity ϵ_M and the bulk electron concentration on the left, $c_{-\infty}$, equals the bulk concentration on the right, c_{∞} ; since $c_{\infty} = c_{-\infty}$, both metals have the Thomas–Fermi length λ_M defined in Eq. 23.

Whereas the electron concentrations on the far left and the far right are similar, the bulk metal's electrostatic potentials (Φ_{bulk} in Eqs. 12 and 14) may differ. The left electrode's dimensionless Fermi level relative to the electrolyte's potential of zero charge will be designated ϕ_{bL} , and the right electrode's, ϕ_{bR} ; two limiting relationships,

$$\lim \phi_L(x) = \phi_{bL} \text{ and } \lim \phi_R(x) = \phi_{bR}, \quad [54]$$

serve as far-field boundary conditions. On either side of the electrolyte domain, the potential and displacement field satisfy the matching conditions

$$\begin{aligned} \phi_L(0) = \phi(0) \text{ and } \phi(L) = \phi_R(L), \\ \epsilon_M \frac{d\phi_L}{dx} \Big|_0 = \epsilon \frac{d\phi}{dx} \Big|_0 \text{ and } \epsilon \frac{d\phi}{dx} \Big|_L = \epsilon_M \frac{d\phi_R}{dx} \Big|_L. \end{aligned} \quad [55]$$

Here we continue to use ϕ to represent the potential distribution in the separating electrolyte.

Auxiliary constraints.—Before stating the governing equations, it is worthwhile to take a step back and consider three auxiliary conditions that physically self-consistent solutions of the two-electrode problem must meet. Most simply, the application of voltage bias by a potentiostat fixes the difference between the electrodes' Fermi levels,

$$\Delta\phi = \phi_{bL} - \phi_{bR}. \quad [56]$$

Also, whatever its electrical state, if an electrolyte domain of finite size has nonreactive boundaries, then the total numbers of anions and cations it contains must be conserved. The two additional auxiliary conditions associated with ion conservation under bias are more conveniently expressed as the conservation of net charge and the conservation of total salt mass.

In the liquid phase, global conservation of net charge requires that

$$\int_0^L \rho_e dx = 0. \quad [57]$$

One can express this as a functional of ϕ by inserting Eq. 16 for ρ_e . Alternatively, put Eq. 6 into condition 57, then apply the divergence theorem to produce

$$\frac{d\phi}{dx} \Big|_0 = \frac{d\phi}{dx} \Big|_L, \quad [58]$$

a simpler relationship to apply in practice.

When describing the electrowetting of liquid/liquid interfaces on metal surfaces, Monroe and colleagues showed how charge conservation constrains the zero-charge potential Φ_{ref} (cf. Eqs. 15–17) of a fixed-volume electrolytic droplet.²³ Within the variational approach of Bazant et al., Φ_{ref} arises as a Lagrange multiplier associated with the application of constraint 57 while minimizing the free-energy functional that applies to the electrolyte phase.¹² These prior observations will manifest differently here because of the choice of reference state for the dimensionless potentials: since Eq. 21 defines the voltage relative to the liquid's potential of zero charge, Φ_{ref} does not appear directly below. Instead, constraint 58 will force an additional relationship—beyond Eq. 56—between the metals' dimensionless Fermi levels.

Global conservation of salt mass in the liquid phase implies the condition

$$\int_0^L c dx = L \langle c \rangle, \quad [59]$$

in which the average local ion concentration c depends on voltage through Eq. 17. Recall also that $\langle c \rangle$, the globally volume-averaged salt concentration in an unbiased equilibrium state, does not necessarily equal c_{ref} , which was formally defined as the salt concentration at a location with zero excess charge density. Generally the concentration of zero excess charge c_{ref} varies with bias, because applied voltage draws ions of both signs out of the bulk of the electrolyte when producing space-charge layers at its edges. As pointed out by both Bazant et al. and Monroe et al.,^{12,13} this implies that the Debye length λ in Eq. 26 must also vary with applied voltage. Analysis of a confined electrolyte can be clarified by instead defining the Debye length in terms of the volume-averaged concentration,

$$\langle \lambda \rangle = \sqrt{\frac{\epsilon RT}{2F^2 z^2 \langle c \rangle}}, \quad [60]$$

which makes it a constant material property of the electrolyte domain. By introducing another dimensionless parameter,

$$\theta = \frac{\lambda}{\langle \lambda \rangle} = \sqrt{\frac{\langle c \rangle}{c_{\text{ref}}}}, \quad [61]$$

one can state auxiliary condition 59 in a clearer way: insert Eqs. 17 and 61 into auxiliary condition 59 to get

$$\frac{1}{L} \int_0^L \cosh(z\phi) dx = \theta^2. \quad [62]$$

This self-consistency constraint extracts the value of θ from the potential distribution, thereby determining the zero-charge

concentration c_{ref} . Since $\cosh(z\phi) \geq 1$ for any ϕ , the concentration of zero charge cannot be greater than the global-average salt concentration. More strictly, c_{ref} must be less than $\langle c \rangle$ whenever $\phi(x)$ does not vanish uniformly. In short, confinement of a liquid electrolyte always elongates its apparent Debye length.

Problem statement.—Across the parallel-plate double-layer capacitor, the potential obeys governing equations

$$\begin{aligned} \lambda_M^2 \gamma \frac{d^2 \phi_L}{dx^2} &= \left[1 - \frac{2}{3} \gamma (\phi_{\text{bL}} - \phi_L) \right]^{3/2} - 1; \quad x < 0, \\ \langle \lambda \rangle^2 \theta^2 z \frac{d^2 \phi}{dx^2} &= \sinh(z\phi); \quad 0 < x < L, \\ \lambda_M^2 \gamma \frac{d^2 \phi_R}{dx^2} &= \left[1 - \frac{2}{3} \gamma (\phi_{\text{bR}} - \phi_R) \right]^{3/2} - 1; \quad x > L. \end{aligned} \quad [63]$$

To find the capacitor's equilibrium electrical state under a voltage bias $\Delta\phi$, one should solve this system subject to far-field boundary conditions 54 and matching boundary conditions 55. After finding a general solution, self-consistent values of the bulk parameters ϕ_{bL} , ϕ_{bR} , and θ in terms of $\Delta\phi$ emerge from the application of auxiliary conditions 56, 58, and 62.

Ultimately, the local mechanical state throughout the capacitor can be computed in terms of the potential distribution, through

$$p(x) - p^\theta = \begin{cases} \frac{1}{6} RT \gamma c_{-\infty} \left(\lambda_M \frac{d\phi_L}{dx} \right)^2; & x < 0, \\ RT z^2 \langle c \rangle \left(\langle \lambda \rangle \frac{d\phi}{dx} \right)^2; & 0 < x < L, \\ \frac{1}{6} RT \gamma c_{\infty} \left(\lambda_M \frac{d\phi_R}{dx} \right)^2; & x > L. \end{cases} \quad [64]$$

As we found when analyzing the semi-infinite capacitive interface above, Korteweg–Helmholtz forces will account for pressure discontinuities at both liquid/metal interfaces.

Perturbation analysis.—This problem is amenable to analytical attack by regular perturbation in bias, following the method from the “Semi-infinite analysis at low bias” section. In the first instance take the total bias to be small, so that the right sides of Eq. 63 can be replaced with Maclaurin expansions like those laid out in Eqs. 42 and 43. This small-bias assumption also allows auxiliary condition 62 to be rewritten as

$$\frac{z^2}{2L} \int_0^L \phi^2 dx + O(\Delta\phi^3) = \theta^2 - 1; \quad [65]$$

auxiliary conditions 56 and 58 retain the same form whatever the size of the bias.

To the list of perturbation-expanded functions in Eq. 40, add

$$\phi_R(x) = \Delta\phi \phi_R^{(1)} + \Delta\phi^2 \phi_R^{(2)} + O(\Delta\phi^3) \quad [66]$$

to describe the potential distribution in the right electrode. Also, to incorporate the auxiliary conditions, include perturbed parameters

$$\begin{aligned} \phi_{\text{bL}} &= \Delta\phi \phi_{\text{bL}}^{(1)} + \Delta\phi^2 \phi_{\text{bL}}^{(2)} + O(\Delta\phi^3), \\ \phi_{\text{bR}} &= \Delta\phi \phi_{\text{bR}}^{(1)} + \Delta\phi^2 \phi_{\text{bR}}^{(2)} + O(\Delta\phi^3), \\ \theta &= 1 + \Delta\phi \theta^{(1)} + \Delta\phi^2 \theta^{(2)} + O(\Delta\phi^3). \end{aligned} \quad [67]$$

The expansion for θ equals 1 at leading order because all the potentials vanish uniformly if $\Delta\phi = 0$.^e

At first order, the perturbed governing system is

$$\begin{aligned} \lambda_M^2 \frac{d^2 \phi_L^{(1)}}{dx^2} &= \phi_L^{(1)} - \phi_{\text{bL}}^{(1)}; \quad x < 0, \\ \langle \lambda \rangle^2 \frac{d^2 \phi^{(1)}}{dx^2} &= \phi^{(1)}; \quad 0 < x < L, \\ \lambda_M^2 \frac{d^2 \phi_R^{(1)}}{dx^2} &= \phi_R^{(1)} - \phi_{\text{bR}}^{(1)}; \quad x > L, \end{aligned} \quad [68]$$

and at second order,

$$\begin{aligned} \lambda_M^2 \frac{d^2 \phi_L^{(2)}}{dx^2} &= \phi_L^{(2)} - \phi_{\text{bL}}^{(2)} + \frac{1}{6} \gamma (\phi_L^{(1)} - \phi_{\text{bL}}^{(1)})^2; \quad x < 0, \\ \langle \lambda \rangle^2 \frac{d^2 \phi^{(2)}}{dx^2} + 2\theta^{(1)} \langle \lambda \rangle^2 \frac{d^2 \phi^{(1)}}{dx^2} &= \phi^{(2)}; \quad 0 < x < L, \\ \lambda_M^2 \frac{d^2 \phi_R^{(2)}}{dx^2} &= \phi_R^{(2)} - \phi_{\text{bR}}^{(2)} + \frac{1}{6} \gamma (\phi_R^{(1)} - \phi_{\text{bR}}^{(1)})^2; \quad x > L. \end{aligned} \quad [69]$$

Being linear, matching conditions 55 are identical at every order of perturbation, taking perturbed forms similar to Eq. 48. Upon perturbation, far-field conditions 54 become

$$\lim_{x \rightarrow -\infty} \phi_L^{(k)}(x) = \phi_{\text{bL}}^{(k)} \quad \text{and} \quad \lim_{x \rightarrow \infty} \phi_R^{(k)}(x) = \phi_{\text{bR}}^{(k)}, \quad [70]$$

with the constant bulk potentials determined at all orders by the perturbed auxiliary condition

$$\phi_{\text{bL}}^{(k)} - \phi_{\text{bR}}^{(k)} = \delta_{1k}. \quad [71]$$

Global charge neutrality of the liquid phase implies a perturbed auxiliary condition that, like the matching conditions, holds at every order,

$$\left. \frac{d\phi^{(k)}}{dx} \right|_0 = \left. \frac{d\phi^{(k)}}{dx} \right|_L. \quad [72]$$

A first-order perturbation of the conservation law for liquid-phase salt mass shows that $\theta^{(1)} = 0$. At second order, the remaining auxiliary condition becomes

$$\frac{z^2}{2L} \int_0^L (\phi^{(1)})^2 dx = (\theta^{(1)})^2 + 2\theta^{(2)} = 2\theta^{(2)}, \quad [73]$$

in which the final equality includes the first-order result.

Solution of the perturbation problem produces results that involve material parameters γ and $\langle \alpha_0 \rangle$, with the latter put in triangular brackets to emphasize its basis on $\langle \lambda \rangle$ (and hence $\langle c \rangle$), rather than λ (or c_{ref}). Also, a new dimensionless geometric parameter appears,

$$\Lambda = \frac{L}{2\langle \lambda \rangle}, \quad [74]$$

which puts the electrode separation in units of two unbiased Debye lengths. We expect that the dielectric limit of behavior should attain when $\Lambda \ll 1$; the electrolytic limit holds when $\Lambda \gg 1$.

Distributions.—We shall see that the perturbed potential distributions depend naturally on the total null-bias differential capacitance of the parallel-electrode cell,

$$\tilde{C}_{\parallel} = \frac{F \Sigma_M^{(1)}}{RT} = \left(\frac{2}{\epsilon_M / \lambda_M} + \frac{2 \tanh \Lambda}{\epsilon / \langle \lambda \rangle} \right)^{-1}. \quad [75]$$

Observe that in the limit $\Lambda \rightarrow \infty$, $\tilde{C}_{\parallel} \rightarrow \frac{1}{2} \langle \tilde{C}_0 \rangle$ —that is, when the electrode spacing is large, the capacitance approaches that of two semi-infinite double-layer capacitances in series. When $\Lambda \ll 1$, on the other hand,

^eSome additional analysis is needed to get $\theta^{(0)}$ if the metal/electrolyte interfaces have inherent surface charges at unbiased equilibrium, a case where $\Delta\phi = 0$ does not require that $\phi_{\text{bL}} = \phi_{\text{bR}} = 0$. Inherently charged surfaces also might require one to revisit matching conditions 55 and auxiliary condition 57. For simplicity we do not consider such situations now, but they may be more realistic.

$$\lim_{\Lambda \ll 1} \tilde{C}_{||} = \left(\frac{2}{\epsilon_M / \lambda_M} + \frac{1}{\epsilon / L} \right)^{-1}. \quad [76]$$

If the electrode spacing is much smaller than the Debye length of the electrolyte, but much more than $2\epsilon/\epsilon_M$ times the Thomas–Fermi length of the electrodes, the system will satisfy the classical expression for dielectric capacitors, $\tilde{C}_{||} \approx \epsilon/L$. Thus the electrostatic model accesses the dielectric limit defined in the preamble.

When electrolytes have large relative permittivity it may be hard to achieve the dielectric limit cleanly in practice, however. For an aqueous solution sandwiched between gold electrodes, the electrode spacing must be much larger than 9.4 nm for the cell capacitance to be unaffected by Thomas–Fermi screening; for the Debye length to greatly exceed 9.4 nm, the salt concentration in water at room temperature must be far less than 1 mM.

Interesting features specific to the parallel-plate configuration appear when $\Lambda = O(1)$, a domain we shall explore after developing dimensionless forms of the potential distributions. To state these more simply it is helpful to introduce a parameter analogous to α , which quantifies the fraction of the potential drop that occurs across the capacitor's separator in the limit of zero bias:

$$\alpha_{||} = 1 - \frac{\tilde{C}_{||}}{\frac{1}{2}\epsilon_M / \lambda_M} = \frac{\langle \alpha_0 \rangle \tanh \Lambda}{1 - \langle \alpha_0 \rangle + \langle \alpha_0 \rangle \tanh \Lambda}. \quad [77]$$

As well as the interfacial property $\langle \alpha_0 \rangle$, which can be computed solely in terms of metal and liquid properties, the partitioning of bias in the two-electrode case also depends on the plate separation, embodied by the geometric quantity Λ . The first equality here emphasizes that the fraction of the potential drop partitioned to the liquid can be found by putting the total cell capacitance in units of two series Thomas–Fermi-layer capacitances.

Together, differential governing systems 68 and 69, accompanied by the perturbed forms of matching conditions 55, far-field conditions 70, and auxiliary conditions 71 to 73, determine the potential distribution throughout the parallel-plate capacitor up to order $\Delta\phi^2$. Incorporation of the relative-capacitance parameter $\alpha_{||}$ into the distribution shows that

$$\begin{aligned} \phi_L &= \frac{1}{2} [1 - (1 - \alpha_{||})e^{x/\lambda_M}] \Delta\phi + \frac{1}{72} \gamma (1 - \alpha_{||})^2 \\ &\quad \times (1 - e^{x/\lambda_M})^2 \Delta\phi^2 + O(\Delta\phi^3); \quad x < 0, \\ \phi &= \frac{\alpha_{||}}{2 \sinh \Lambda} \sinh \left(\Lambda - \frac{x}{\langle \lambda \rangle} \right) \Delta\phi + O(\Delta\phi^3); \quad 0 < x < L, \\ \phi_R &= -\frac{1}{2} [1 - (1 - \alpha_{||})e^{(L-x)/\lambda_M}] \Delta\phi \\ &\quad + \frac{1}{72} \gamma (1 - \alpha_{||})^2 (1 - e^{(L-x)/\lambda_M})^2 \\ &\quad \times \Delta\phi^2 + O(\Delta\phi^3); \quad x > L. \end{aligned} \quad [78]$$

Here the first-order perturbations of the potentials are similar to those found in the "Semi-infinite analysis at low bias" section, with α_0 replaced by $\alpha_{||}$ and half the bias apportioned to each interface.^f The second-order terms in the expansions differ substantially from expectations set by Eq. 49, however.

Figure 6 shows potential distributions across the ideal parallel-plate electrolytic capacitor for plate separations ranging from 2 Debye lengths ($\Lambda = 1$) up to 200 Debye lengths ($\Lambda = 100$). (A lower electrolyte concentration of 0.5 mM was used when making this figure, to partition more of the applied bias to the separator domain.) When the plate separation is much smaller than the Debye length, the number of charge carriers in the electrolyte is too low to screen the electrodes' surface charges. The field between the electrodes therefore remains essentially constant, so the potential varies linearly across the liquid phase, as one would expect in a dielectric capacitor.

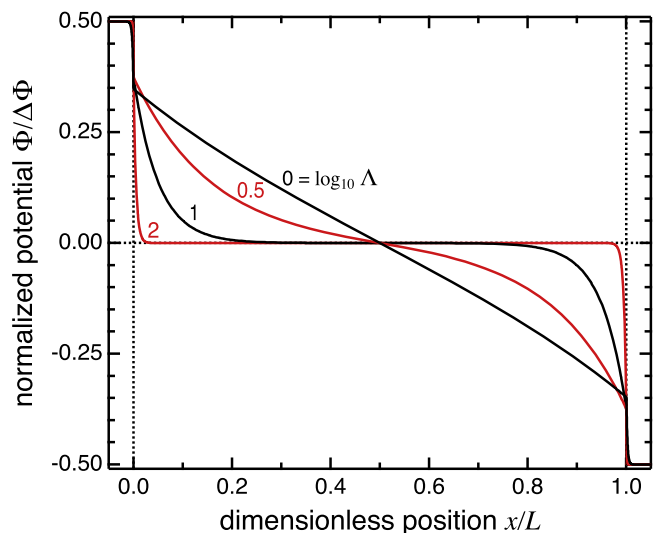


Figure 6. Potential distribution in an ideal parallel-plate capacitor with gold/0.5 mM aqueous NaCl interfaces ($\gamma = 0.007$, $\langle \alpha_0 \rangle = 0.75$, $\lambda_M / \langle \lambda \rangle = 0.0042$) biased at $\Delta\phi = 0.25$ with plate separations ranging from $\Lambda = 1$ to 100.

With much larger plate separation, the number of carriers suffices to facilitate complete charge screening. The field decreases rapidly within thin layers near the electrode surfaces, leading to a corresponding steep change in potential, and vanishes in the bulk of the separator, where the potential plateaus to a constant value. The model interpolates naturally between dielectric and electrolytic extremes. When the plates are around six Debye lengths apart ($\Lambda = \sqrt{10} \approx 3.2$), there is a mixed response, where some screening effect is observable, but a field still penetrates through the point of zero excess charge density halfway across the cell.

Differences between second-order terms of the potential distributions in Eqs. 49 and 78 can be understood by examining the self-consistent parameters obtained from the parallel-plate analysis:

$$\begin{aligned} \phi_{bL} &= \frac{1}{2} \Delta\phi + \frac{1}{72} \gamma (1 - \alpha_{||})^2 \Delta\phi^2 + O(\Delta\phi^3), \\ \phi_{bR} &= -\frac{1}{2} \Delta\phi + \frac{1}{72} \gamma (1 - \alpha_{||})^2 \Delta\phi^2 + O(\Delta\phi^3), \\ \theta &= 1 + \frac{1}{32} z^2 \alpha_{||}^2 \left(\frac{\coth \Lambda}{\Lambda} - \text{csch}^2 \Lambda \right) \Delta\phi^2 + O(\Delta\phi^3). \end{aligned} \quad [79]$$

Constraints expressing the conservation of ions require that when applied voltage increases, the liquid's potential of zero charge must shift downward relative to the bulk Fermi levels of both metal electrodes, as shown by the second-order terms in ϕ_{bL} and ϕ_{bR} . When ions move away from the bulk to screen surface charges at the electrolyte's boundaries, the electrolyte's concentration of zero excess charge also falls, leading to the second-order term in θ . In contrast, the semi-infinite analysis provided no route by which the potential or concentration of zero charge could change, so higher-order screening effects in the metal had to be compensated by changing the shape of the potential distribution on the liquid side of the interface.

The local pressure is found by inserting Eq. 78 into Eq. 64. Up to the second order of perturbation,

$$\frac{p^{(2)}(x)}{\langle p_0 \rangle} = \begin{cases} \sqrt{\frac{1 - \langle \alpha_0 \rangle}{\langle \alpha_0 \rangle \lambda_M / \langle \lambda \rangle}} \left[\frac{(1 - \alpha_{||})e^{x/\lambda_M}}{2(1 - \langle \alpha_0 \rangle)} \right]^2; & x < 0, \\ 3 \sqrt{\frac{\langle \alpha_0 \rangle \lambda_M / \langle \lambda \rangle}{1 - \langle \alpha_0 \rangle}} \left[\frac{\alpha_{||} \cosh \left(\frac{x}{\langle \lambda \rangle} - \Lambda \right)}{2 \langle \alpha_0 \rangle \sinh \Lambda} \right]^2; & 0 < x < L, \\ \sqrt{\frac{1 - \langle \alpha_0 \rangle}{\langle \alpha_0 \rangle \lambda_M / \langle \lambda \rangle}} \left[\frac{(1 - \alpha_{||})e^{(L-x)/\lambda_M}}{2(1 - \langle \alpha_0 \rangle)} \right]^2; & x > L, \end{cases} \quad [80]$$

which is plotted for a capacitor with gold electrodes separated by 0.05 M aqueous NaCl on Fig. 7. In the main panel, the vertical scale

^fNote that $\lim_{\Lambda \rightarrow \infty} \sinh(\Lambda - x/\langle \lambda \rangle) / \sinh(\Lambda) = \exp(-x/\langle \lambda \rangle)$ and $\lim_{\Lambda \rightarrow \infty} \sinh[-\Lambda + (L - x)/\langle \lambda \rangle] / \sinh(\Lambda) = -\exp[(x - L)/\langle \lambda \rangle]$.

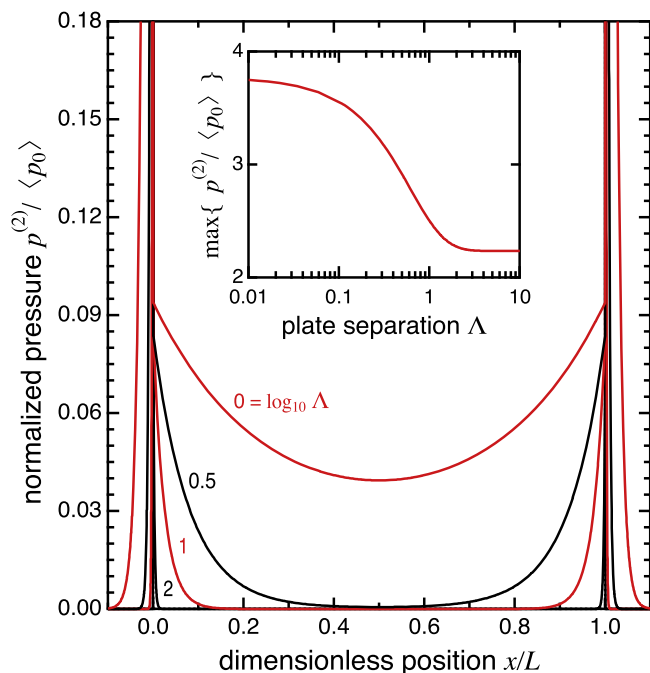


Figure 7. Second-order gauge pressure correction in an ideal parallel-plate capacitor with gold plates separated by 0.05 M aqueous NaCl ($\gamma = 0.007$, $\langle\alpha_0\rangle = 0.23$, $\lambda_M/\langle\lambda\rangle = 0.042$) with plate separations ranging from $\Lambda = 1$ to 100. Inset: variation of the maximum pressure, which is achieved on the gold sides of both gold/electrolyte interfaces, with plate separation.

has been magnified to illustrate the behavior within the separator, since the scale of electrolyte pressure differs from the electrode pressure by a factor of $3\epsilon_M/\epsilon$. The maximum pressure, plotted in the inset panel, occurs on the gold sides of the gold/electrolyte interfaces. Although maximum pressure has a sigmoidal shape with respect to plate separation, it drops by less than a factor of 2 between the dielectric and electrolytic extremes.

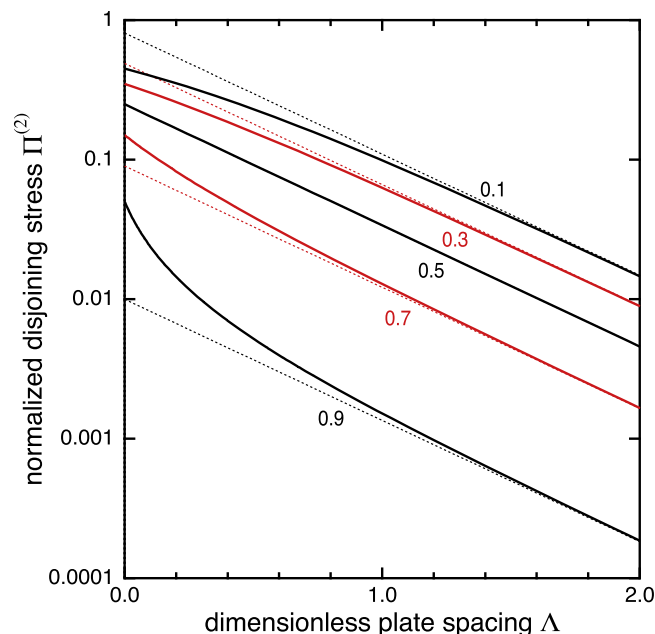


Figure 8. Second-order disjoining-stress correction as a function of separation distance Λ for parallel-plate dielectric capacitors with null-bias partition coefficients $\langle\alpha_0\rangle$ ranging from 0.1 to 0.9. The dotted lines show responses expected from Verwey-Overbeek theory.

Disjoining stress.—We are finally in a position to determine what force—if any—attracts the capacitor's plates together, i.e. the disjoining stress. Through Eq. 5, disjoining stress will manifest as a net force that pulls the electrodes together, which will be compensated by the coil springs in Fig. 1. To quantify this attraction, one must distinguish local forces, which squeeze space-charge layers together near each interface, from the externally observable force that draws one electrode toward the other. Charge screening generally reduces this external force; compressive stress concentrates near the interface, but does not penetrate across the electrolyte.

Only the unscreened portion of the field, that is, the portion of the field that exists along the surface of zero excess charge density within the separator, pulls the electrodes together. In the present situation, for reasons of symmetry, said surface resides at $x = L/2$, halfway across the cell. Bearing in mind Eq. 20, the gauge stress there is found through Eq. 80, after substantial rearrangement and simplification involving Eqs. 21, 23, 51, 53, 60, and 77, to be

$$(\sigma_{xx} - p^\theta)|_{L/2} = \frac{1}{2\epsilon} \left(\frac{\tilde{C}_\parallel \Delta \Phi}{\cosh \Lambda} \right)^2 + O(\Delta \phi^2), \quad [81]$$

in which Eq. 75 can be used to show that

$$\begin{aligned} \frac{\tilde{C}_\parallel}{\cosh \Lambda} &= \frac{\frac{\epsilon}{L}}{\frac{2\epsilon}{\epsilon_M} \cdot \frac{\lambda_M}{L} \cosh \Lambda + \frac{\sinh \Lambda}{\Lambda}} + O(\Delta \phi^2) \\ &= \frac{\langle \tilde{C}_0 \rangle e^{-\Lambda}}{1 - (2\langle \alpha_0 \rangle - 1)e^{-2\Lambda}} + O(\Delta \phi^2). \end{aligned} \quad [82]$$

The first of these expressions is useful to assess asymptotic behavior when the Debye length $\langle\lambda\rangle$ is very large compared to the plate spacing, i.e. in the limit $\Lambda \ll 1$; the second is useful when $\langle\lambda\rangle \ll L$, so that $\Lambda \gg 1$.

Away from the regime where $\lambda_M \ll L$ and $L \ll \langle\lambda\rangle$, the dimensionless disjoining stress $\Pi^{(2)}$ can be written as

$$\Pi^{(2)} = \frac{8\epsilon\lambda_M^2 F^2 \sigma_{xx}^{(2)}|_{L/2}}{\epsilon_M^2 R^2 T^2} = \frac{(1 - \langle\alpha_0\rangle)^2 e^{-2\Lambda}}{[1 - (2\langle\alpha_0\rangle - 1)e^{-2\Lambda}]^2}. \quad [83]$$

This result confirms the observation by Israelachvili, and before him, Verwey and Overbeek, that the electrostatic interaction between two charged surfaces should decay exponentially with their separation distance; the rate of decay is determined by the Debye length.^{24,25} Our model shows that at moderate separation distances (when $\Lambda \sim 1$), the electrostatic disjoining stress can deviate from exponential decay because of Thomas-Fermi screening within the electrode itself. This effect is present even in the linear theory (first-order perturbation).

The disjoining pressure generally depends on $\langle\alpha_0\rangle$, and is illustrated as a function of plate separation in Fig. 8. Observe that $\langle\alpha_0\rangle$ tends toward unity when $\langle\lambda\rangle \gg \lambda_M$ —in this instance, electrostatics suggests that higher-than-expected disjoining pressures should be observed. Upward deviation from exponential decay as plates grow nearer to each other is commonly seen in experiments with the surface force balance,²⁶ the analysis of which may in future shed light on the role of the solid substrate.

Last, one can insert the first of expressions 82 into Eq. 81 to show that

$$\lim_{\Lambda \rightarrow 0} \lim_{\lambda_M/L \rightarrow 0} (\sigma_{xx} - p^\theta)|_{L/2} = \frac{\epsilon \Delta \Phi^2}{2L^2} + O(\Delta \phi^3). \quad [84]$$

Thus the model reproduces the standard formula for the force between plates of a dielectric capacitor, as Dr. Biggins suggested it should.

Outlook

A few new phenomena and scaling laws have been elucidated by this extended electrostatic theory, which considers electronic

structure within the electrode surface as well as charge screening in the adjacent electrolyte. Several motivating questions about the interelectrode forces and stresses within electrolytic capacitors were resolved. The theory shows that charge accumulation in a double layer always produces compressive gauge stresses, which peak at the interface and decay with respect to distance on either side of it. Underscreening of the field in the separating electrolyte can result in an externally observable interelectrode force, which manifests as a disjoining pressure. In the limit that the Thomas–Fermi length is very small compared to the plate separation and the plate separation is very small compared to the Debye length, the disjoining pressure achieves the value expected for a traditional dielectric capacitor. Away from this regime, the disjoining pressure decays exponentially as the electrodes are drawn apart.

The idealization of the system presented here helped to illustrate basic scaling laws, and also allowed us to clearly outline a broadly applicable analytical approach. Applications to practical electrolytic capacitors probably require several more detailed considerations. Straightforward modification of the theory could be made to account for inherently charged interfaces, which would produce a repulsive contribution to the disjoining pressure in a symmetric cell. It should also be possible to include more realistic physics, such as detailed band structures of the electrodes and entropic effects arising from van der Waals forces, by accounting for nonideality in the electrochemical constitutive laws that relate carrier concentrations to potential (and possibly pressure). A coupled Cauchy–Poisson analysis, which considers the finite bulk moduli and composition-dependent density of the materials making up the capacitor, could be enlightening.

Acknowledgments

This work was supported by the Faraday Institution, subawards FIRG003 and FIRG007 under EPSRC grant no. EP/S003053/1, and the ISCF Materials Research Hub for Energy Conversion, Capture, and Storage (M-RHEX), grant no. EP/R023581/1.

References

1. L. Onsager, "Theories and problems of liquid diffusion." *Annals of the New York Academy of Sciences*, **46**, 241 (1945).
2. S. R. de Groot, "Thermodynamics of Irreversible Processes." (Interscience Publishers, New York) (1951).
3. S. R. de Groot and P. Mazur, "Non-Equilibrium Thermodynamics." (North-Holland, Amsterdam) (1962).
4. A. Kornyshev and M. A. Vorotyntsev, "Conductivity and space-charge phenomena in solid electrolytes with one mobile charge carrier species, a review with original material." *Electrochim. Acta*, **26**, 303 (1981).
5. S. Braun, C. Yada, and A. Latz, "Thermodynamically consistent model for space-charge-layer formation in a solid electrolyte." *J. Phys. Chem. C*, **119**, 22281 (2015).
6. P. Goyal and C. W. Monroe, "New foundations of Newman's theory for solid electrolytes: thermodynamics and transient balances." *J. Electrochem. Soc.*, **164**, E3647 (2017).
7. J. Newman and K. E. Thomas-Alyea, "Electrochemical Systems." (John Wiley & Sons, Inc., Hoboken, New Jersey) 3rd ed. (2004).
8. G. Li and C. W. Monroe, "Dendrite nucleation in lithium-conductive ceramics." *Phys. Chem. Chem. Phys.*, **21**, 20354 (2019).
9. C. W. Monroe, "Current-induced stresses in ceramic lithium-ion conductors." in *Engineering Department Bio- and Micromechanics Seminar* (University of Cambridge, UK) (2018), <http://talks.cam.ac.uk/talk/index/97735>.
10. D. L. Chapman, "A contribution to the theory of electrocapillarity." *Philos. Mag.*, **25**, 475 (1913).
11. D. C. Grahame, "The electrical double layer and the theory of electrocapillarity." *Chem. Rev.*, **41**, 441 (1947).
12. M. Z. Bazant, K. Thornton, and A. Ajdari, "Diffuse-charge dynamics in electrochemical systems." *Phys. Rev. E*, **70**, 021506 (2004).
13. C. W. Monroe, M. Urbakh, and A. A. Kornyshev, "The distinctive electrowetting properties of ITIES." *J. Phys.: Condens. Matter*, **19**, 375113 (2007).
14. R. B. Bird, W. E. Stewart, and E. N. Lightfoot, "Transport Phenomena." (John Wiley & Sons, New York) (1958).
15. A. A. Kornyshev, W. Schmickler, and M. A. Vorotyntsev, "Nonlocal electrostatic approach to the problem of a double-layer at a metal-electrolyte interface." *Phys. Rev. B*, **25**, 5244 (1982).
16. W. D. Ristenpart, I. A. Aksay, and D. A. Saville, "Assembly of colloidal aggregates by electrohydrodynamic flow: kinetic experiments and scaling analysis." *Phys. Rev. E*, **69**, 021405 (2004).
17. J. Liu and C. W. Monroe, "Solute-volume effects in electrolyte transport." *Electrochim. Acta*, **135**, 447 (2014).
18. J. R. Melcher, "Continuum Electromechanics." (MIT Press, Cambridge, United States of America) (1981).
19. O. K. Rice, "Application of the Fermi statistics to the distribution of electrons under fields in metals and the theory of electrocapillarity." *Phys. Rev.*, **31**, 1051 (1928).
20. N. W. Ashcroft and N. D. Mermin, "Solid State Physics." (Saunders College Publishing, Philadelphia, United States of America) (1976).
21. D. C. Grahame, "Differential capacity of mercury in aqueous sodium fluoride solutions 1. Effect of concentration at 25 degrees." *J. Am. Chem. Soc.*, **76**, 4819 (1954).
22. O. Stern, "Zur Theorie der elektrolytischen Doppelschicht." *Z. Elektrochem.*, **30**, 508 (1924).
23. C. W. Monroe, L. Daikhin, M. Urbakh, and A. A. Kornyshev, "Principles of electrowetting with two immiscible electrolytic solutions." *J. Phys.: Condens. Matter*, **18**, 2837 (2006).
24. J. Israelachvili, "Solvation forces and liquid structure, as probed by direct force measurements." *Acc. Chem. Res.*, **20**, 415 (1987).
25. E. J. W. Verwey and J. T. G. Overbeek, "Theory of the Stability of Lyophobic Colloids." (Elsevier, Amsterdam) (1948).
26. A. M. Smith, A. A. Lee, and S. Perkin, "The electrostatic screening length in concentrated electrolytes increases with concentration." *J. Phys. Chem. Lett.*, **7**, 2157 (2016).